Supramolecular effects on the potential of redox units—nanoscaffolds internally functionalised with ferrocene units†

Michael Schmittel,*[a] Bice He,[a] Venkateshwarlu Kalsani[a] and Jan W. Bats[b]

Received 9th March 2007, Accepted 4th June 2007
First published as an Advance Article on the web 26th June 2007
DOI: 10.1039/b703633g

Redox-active nanoscale racks and nanoladders were prepared as proof of principle in a directional heteroleptic approach towards internally functionalised aggregates. Using the HETTAP concept, zinc(II) phenanthroline terpyridine nanoladder and nanorack structures with internal ferrocene units were prepared. Proximal effects exerted by the ferrocene units in the nanoladders could be read out by comparison of their redox potentials with those of nanorack **R1** and of the parent ligand. The increasing compression of the ferrocene units when going from the larger nanoladder **L1** to the smaller aggregate **L2** manifested itself in an enlarged anodic shift. Thus, the redox potential series (*vs.* DMFc: $E_{1/2} = 0.462$ V for **R1**, 0.480 V for **L1** and 0.491 V for **L2**) reveals convincingly the supramolecular effect on a redox transition. At cathodic potentials the zinc(II) phenanthroline terpyridine complexes were decomposed due to a reduction of the ligands, as could be detected from an evaluation of the ferrocene redox potential.

Introduction

Due to their great potential as novel redox-active, catalytic, optical, and mechanical materials,[1] the construction of functional supramolecular assemblies is a topic of current interest.[2,3] While over the years substantial progress has been made to fabricate impressive structures,[4] the focus has recently turned towards the interplay of energy- and electron-harvesting units, such as multiple chromophore or redox relay systems, in supramolecular aggregates.[5,6] As indicated in Scheme 1, metallosupramolecular assemblies are usually constructed by one of two main strategies in order to set up polyfunctional aggregates. For some time, approach A, positioning functional units as ligands on the metal fragments, was the method of choice, mainly due to its simplicity and flexibility.[7] More recently, Hupp,[8] Lehn,[9] Stang,[10] and Würthner[11] have explored approach B1 leading to square motifs, in which functional units were introduced along with the organic spacer ligands. However, due to free rotation[11c] about the central ligand axis these examples[11] lack any directionality, as either external or internal positions may be occupied. As a way out, functional units were placed both externally and internally (Scheme 1; eqn (2)). The problem is better addressed by the directional approach B2 developed by Fujita *et al.*[12] Using the concept depicted in eqn (3), they have prepared diverse 3D self-assembled spherical complexes with endohedral functional units. To supplement this, we now disclose strategy B2, eqn (4), providing a way of incorporating highly-aligned functional units into ladder motifs.[13] This approach, requiring heteroleptic aggregation, goes along with a conformational re-orientation of the functional units in the linear ligand.

Recently, we have developed a strategy for multicomponent ladder assemblies using the HETTAP (HETeroleptic Terpyridine And Phenanthroline complexes) concept,[14] which was used to engineer 2-dimensional nanoscaffolds[14,15] with 2D cavities ≥290 Å^2. The nanoscaffolds were readily prepared from linear shielded bisphenanthrolines[16] and linear bisterpyridines[15] in the presence of various metal ions, such as Zn^{2+}, Cu^{+}, and Hg^{2+}. As this concept provides an entry both to multicomponent aggregates[17] whose size can be varied depending on the length of the ligands, and to directional attachment of various internal units (Scheme 1; eqn (4)), we decided to explore its use for the preparation of nanoscaffolds functionalised internally with redox relays. Based on this conception, two nanoladders of different size were prepared from bisphenanthroline **5** carrying two ferrocene units and from bis-terpyridines **6** and **7** of varying length (Chart 1). Ferrocene was chosen as a redox-active building block in **5** due to its well defined redox properties. A flexible linkage was incorporated to ensure some degree of self-organisation of the ferrocene group. The length of the linkage was optimised from force field modelling of the ladder structures. Accordingly, ferrocene units attached to a hexamethylene linker should allow for easy arrangement within the cavity of the suggested nanoscaffold **L2** (see Fig. 1). Filling the cavity with redox-active units should enable us to investigate the supramolecular effect on the redox potential.[18]

Results and discussion

Synthesis of ligand 5

As a starting point for the preparation of the ferrocene-containing bisphenanthroline **5** we resorted to phenanthroline **1** (Scheme 2).[19] After removal of both protecting groups using 3 N KOH as base, phenanthroline **2** was afforded in 89% yield. Following

[a]*Center of Micro- and Nanochemistry and Engineering, Organische Chemie, Universität Siegen, Adolf-Reichwein-Strasse, 57068 Siegen, Germany. E-mail: schmittel@chemie.uni-siegen.de; Fax: +49 271-740-3270*
[b]*Institute für Organische Chemie und Chemische Biologie, Johann Wolfgang Goethe-Universität, Marie-Curie-Strasse 11, D-60439, Frankfurt am Main, Germany*

† Electronic supplementary information (ESI) available: Numbering of formulae for NMR assignments; NMR spectra; crystal data for **5**; 3D structure representations. See DOI: 10.1039/b703633g

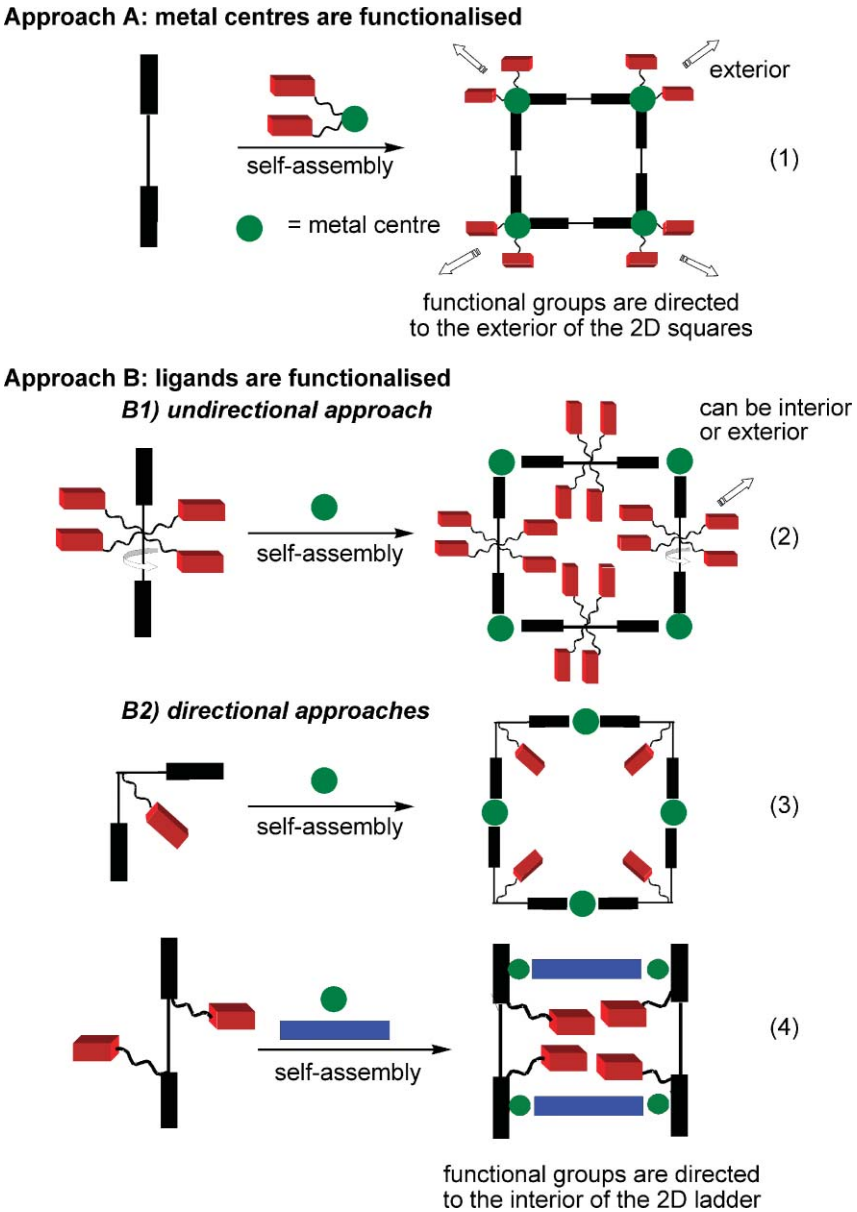

Scheme 1 Cartoon representation of the various approaches currently used for setting up supramolecular aggregates with functional units.

a Sonogashira cross-coupling protocol with $[Pd(PPh_3)_2Cl_2]$ and CuI, the desired bisphenanthroline **3** was always accompanied by a minor amount of the homo-coupling product of **2** (5%), which caused major problems in the chromatographic purification. Luckily, when $[Pd(PPh_3)_4]$ was used as catalyst system, **3** was afforded in 90% yield after purification. Finally, a double Williamson reaction of 1-(6-bromohexyl)ferrocene (**4**)[20] with **3** generated the bisferrocene-functionalised bisphenanthroline **5** in 80% yield.

X-Ray structure of 5

Following a full (NMR, IR, MS) solution-state characterisation, the formation of single crystals obtained by slow evaporation of a DCM–acetonitrile (9 : 1) solution of **5** allowed for an X-ray crystallographic analysis. Due to its conformational flexibility, **5** was present in a transoid conformation in the solid state. As depicted in Fig. 2, the two ferrocene groups are well separated, exhibiting a distance between the two iron atoms of 2.95 nm. The structure is centrosymmetric with a centre of inversion at the midpoint of the central benzene ring. The distance of the two terminal phenanthrolines is 1.75 nm. The crystal packing shows a number of weak intermolecular C–H $\cdots$ π interactions.

Self-assembly of the ferrocene nanoladders L1 and L2 based on the HETTAP concept

With ligand **5** at hand and ligands **6–8** available through earlier work[15] and commercial suppliers, all ingredients for the HETTAP synthesis[14] were available. The synthesis of ladders **L1** ($[Zn_4(\mathbf{5})_2(\mathbf{6})_2)]^{8+}$) and **L2** ($[Zn_4(\mathbf{5})_2(\mathbf{7})_2)]^{8+}$) and rack **R1** ($(Zn(\mathbf{5})(\mathbf{8})_2)]^{4+}$) was readily accomplished by treating (for example, in the case of **L1**) 1 equiv. of **6** with a mixture of 1 equiv. of **5** and 2 equiv. of $Zn(CF_3SO_3)_2$ in DCM–methanol (8 : 2) (Scheme 3).

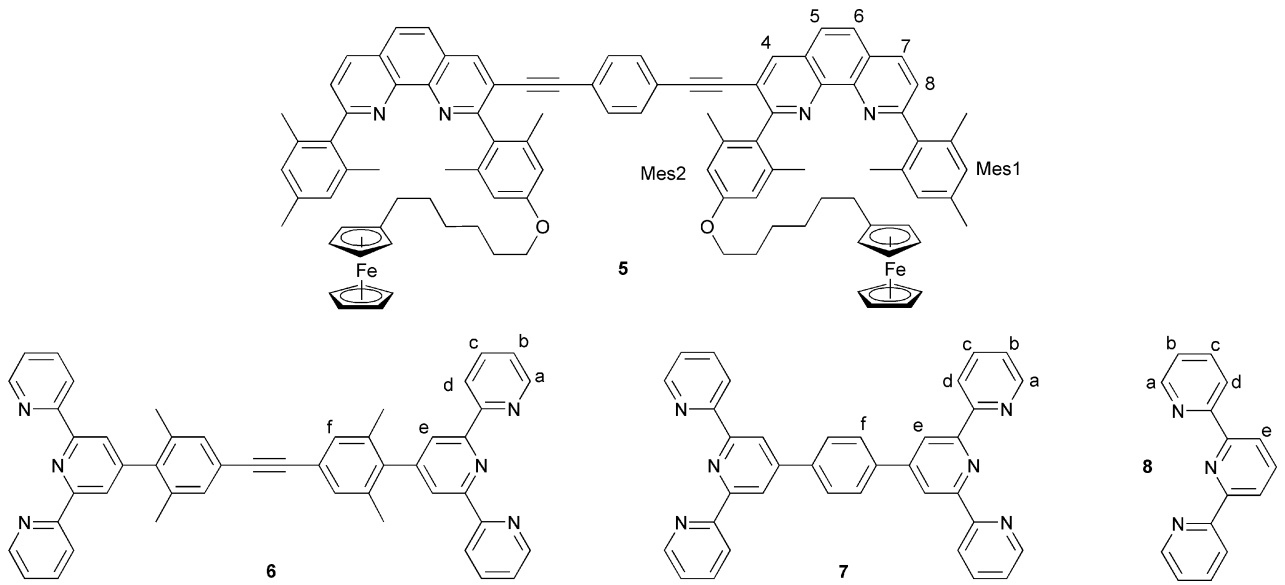

Chart 1 Ligands used in the present study.

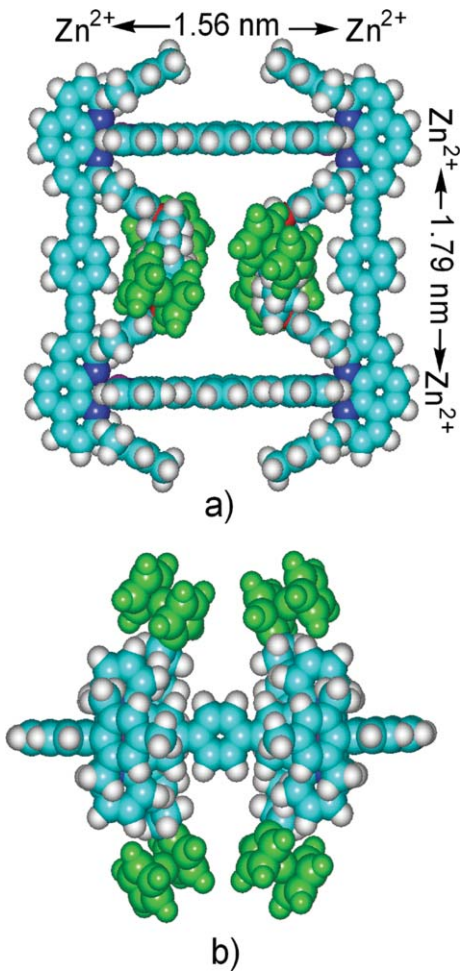

Fig. 1 Side (a) and top (b) views of space-filling presentations of nanoladder **L2** $[Zn_4(\mathbf{5})_2(\mathbf{7})_2)]^{8+}$ as generated from force field modelling (HyperChem®). The atoms/groups are colour coded for clarity: carbon: cyan; nitrogen: blue; oxygen: red; zinc: (hidden); ferrocene group: green.

All ^{1}H NMR spectral data point to the successful formation of **R1**, **L1** and **L2**. For example, the spectra of **L1** and **L2** in CD_2Cl_2–CD_3OD (8 : 2) (see ESI†) showed only one set for each ligand, suggesting that a single species was obtained. Characteristic upfield shifts of the mesityl protons (from $\delta \sim 6.7$ and 6.9 ppm in **5** to 5.8 and 6.2 ppm in **R1**, to 5.9 and 6.3 ppm in **L1**, and to 5.9 and 6.2 ppm in **L2** (see Table 1) and downfield shifts of the phenanthroline protons ($\Delta\delta \sim 1.0$ ppm) are in strong support of the formation of the phen-Zn(II)-terpy complex units. Upon complexation, the ^{1}H NMR signals of the ferrocenyl protons for **R1** and **L1** were shifted slightly downfield from $\delta = 4.08$ to 4.22 and 4.24 ppm, respectively, but the splitting patterns changed dramatically in both cases. In contrast, the signals of ferrocenyl protons in **L2** showed that the splitting pattern was similar to that of **5**, except that the 10‴-H were shifted upfield slightly rather than downfield by 0.22 ppm.

Rewardingly, the ESI-MS spectra of **L1** and **L2** showed the complete pattern of signals corresponding to 3+ to 8+ charged species of **L1** (Fig. 3) and **L2**, with the isotopic distribution of all fragments exactly matching with the calculated ones after loss of the counter-anions.

Electroanalytical investigations

While the combination of the spectroscopic data furnished strong evidence for the proposed structures of **L1** and **L2**, direct proof for supramolecular interaction between ferrocene groups were derived

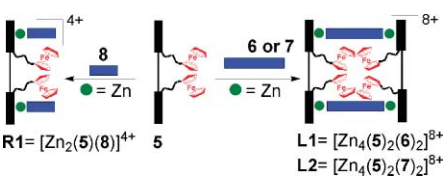

Scheme 3 Cartoon representation of the preparation of nanorack **R1** and nanoladders **L1** and **L2**.

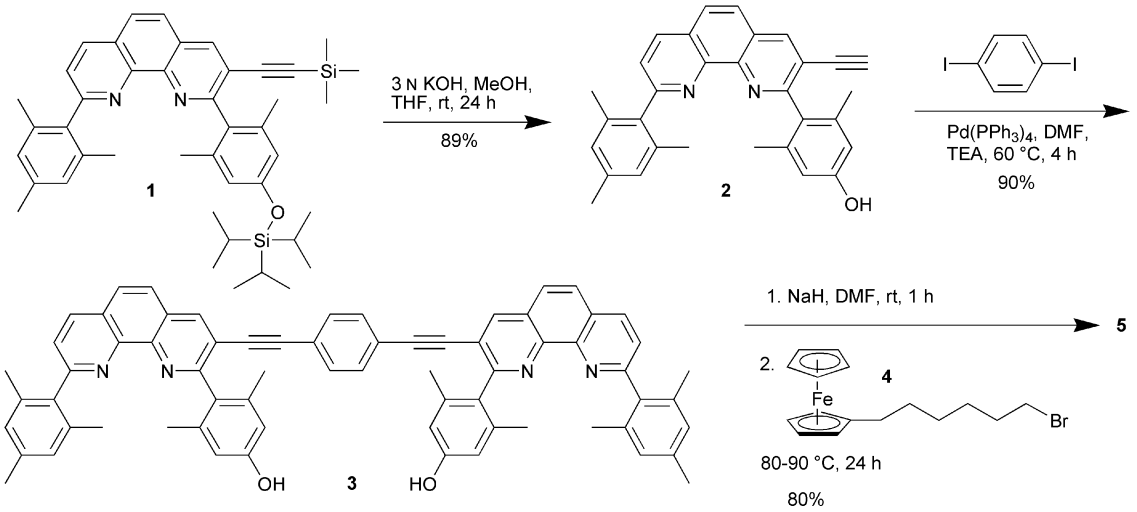

Scheme 2 Preparation of **5**.

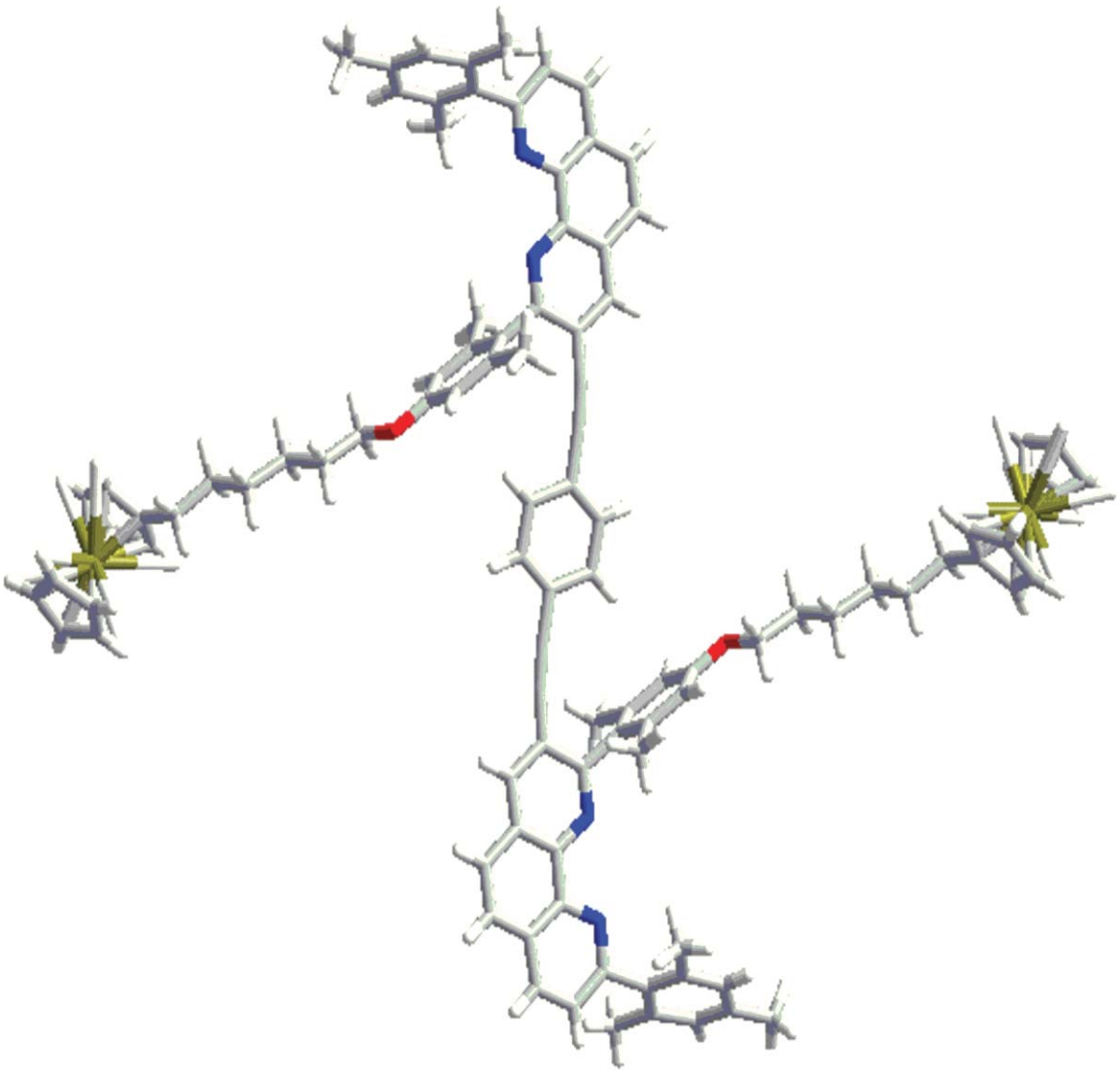

Fig. 2 Molecular structure of the ferrocene-appended rigid bisphenanthroline **5** as a stick representation. Carbon: gray, hydrogen: white, nitrogen: blue, oxygen: red, iron: yellow. CCDC reference number 639848. For crystallographic data in CIF or other electronic format see DOI: 10.1039/b703633g

Table 1 ^{1}H NMR shifts (in ppm, in CD_2Cl_2–CD_3OD (8 : 2) at 400 MHz) of the ligand **5** and nanoscaffolds **R1**, **L1** and **L2**

	Bisphenanthroline protons					Ferrocene protons		
Compound	Mes2-H (s)	Mes1-H (s)	8-H (d)	7-H (d)	4-H (s)	8‴,9‴-H (m)		10‴-H (s)
5[a]	6.67	6.94	7.57	8.33	8.49	4.01–4.07		4.08
Rack **R1**	5.86	6.18	8.03	9.04	9.07		4.22 (br s)	
Ladder **L1**	5.93	6.27	8.05	9.08	9.16		4.24 (br s)	
Ladder **L2**	5.91	6.21	8.09	9.09	9.21	3.92–3.98		3.86

[a] In CD_2Cl_2.

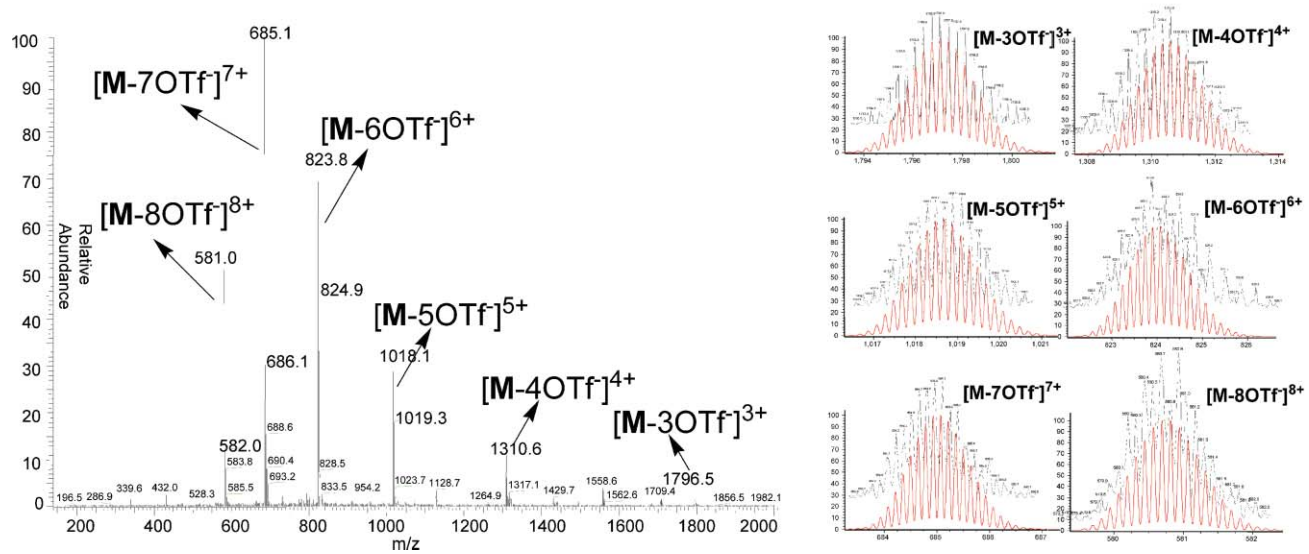

Fig. 3 Left: ESI-MS spectrum of the nanoladder **L1**. Right: Isotopic distributions in the ESI-MS of **L1** (black = experimental, red = calculated) showing all charged species from 3+ to 8+.

from cyclic voltammetry (CV) and differential pulse voltammetry (DPV) investigations.

All measurements were performed in acetonitrile using decamethylferrocene (DMFc) as internal standard. In contrast to Würthner's squares, for which a peak splitting of redox wave of ferrocene units had been reported, suggesting the presence of internal and external ferrocene units,[11] a single oxidation wave was observed for the $Fc^{0,+}$ couple in **4**, **R1**, **L1** and **L2** in CV measurements (Fig. 4). This result suggests that ferrocene units in the various structures are all placed in identical environments on the time scale of the experiment.[21] As indicated in Table 2, the ferrocene unit of **4** shows an oxidation potential of 0.451 V_{DMFc}, while that of **R1** is 0.463 V_{DMFc}. This small anodic shift[22] of 12 mV is most likely caused by formation of the phen-Zn(II)-terpy coordination unit, which ought to have some influence on the ferrocenes' oxidation potential. Less likely is an intramolecular interaction of the two ferrocene units, as we expect the conformation of **R1** to correspond to that of **5**. Accordingly, the ferrocenes should be separated by 3 nm. The oxidation of the ferrocenes in ladders **L1** and **L2** (0.483 V_{DMFc} and 0.487 V_{DMFc}) was effected at higher anodic potentials (20–24 mV) than that in **R1**. The anodic shift is attributed to the ladder structure, which should lead to a compression of the four ferrocenes inside its inner void. As a result, the "intramolecular" interaction of ferrocenes should become perceptible. From the molecular structure of **5**, we derive a distance between the two ferrocene iron atoms of 29.5 Å. Assuming that

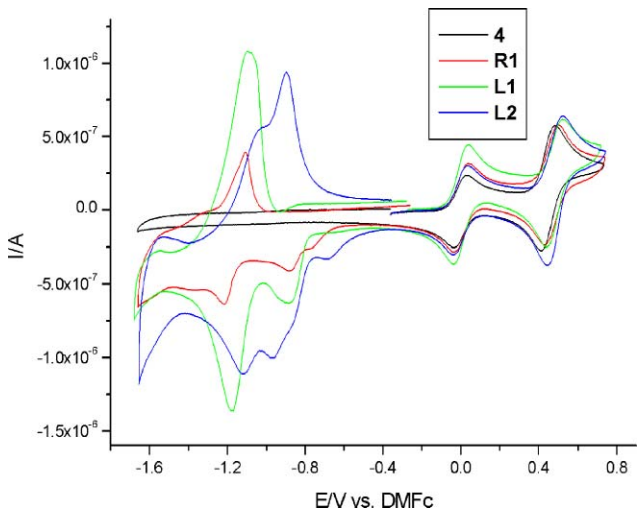

Fig. 4 CVs of compound **4**, **R1**, **L1** and **L2** recorded in 0.10 M ^{n}Bu$_4$NPF$_6$ in acetonitrile at a scan rate of 100 mV s^{-1}.

R1 has the same conformation as **5**, the two ferrocene units in **R1** should be separated by the same distance. Evaluation of the average distances of the four ferrocene iron atoms in the two phen-Zn(II)-terpy ladders as obtained from HyperChem® energy-minimised structures provided values of 18.5 Å and 15.2 Å for **L1** and **L2**, respectively (see ESI† and Fig. 1). The short average

Table 2 Reversible redox potentials of compounds *vs.* DMFc by cyclic voltammetry at a scan rate 100 mV s^{-1}

Compound	$E_{1/2}^{ox}$ ($Fc^{2+/3+}$)	ΔE_p	$E_{1/2}^{red}$ ($terpy^{0/-}$)	ΔE_p
4	0.451 V	68 mV	N/A	N/A
R1	0.463 V	67 mV	−1.162 V	110 mV
L1	0.483 V	87 mV	−1.135 V	88 mV
L2	0.487 V	77 mV	−1.079 V, −0.941 V	94 mV, 64 mV

distance between the four iron atoms in **L1** and **L2** is enforced by the supramolecular framework and should be the dominating effect for the above-described anodic shifts.

DPV investigations on compounds **4**, **R1**, **L1** and **L2** provided further strong support for the above hypothesis (Table 3). When the voltage was scanned from −0.30 V to 1.00 V, the peak values corresponding to ferrocene units in **4**, **R1**, **L1** and **L2** were 0.452, 0.462, 0.480 and 0.491 V_{DMFc}, respectively (Fig. 5). These results are in perfect agreement with those from CV measurements. Intriguingly, upon recording DPVs for **4** and **R1** from −1.60 V to 1.00 V, the oxidation potentials of ferrocene units for both compounds nearly coincided at 0.452 and 0.454 V, respectively. Clearly, the *ca.* 10 mV anodic shift observed for **R1** as compared to **4**, attributed to the formation of the phen-Zn(II)-terpy coordination unit, has disappeared in this experiment. This suggests, that upon starting the measurement at −1.60 V, the terpyridine unit of **R1** is reduced, leading to a dissociation of the coordination complex, which is not repaired on the DPV time scale. As a consequence, the released ligand **5** is then detected in the DPV of **R1**, quite obviously exhibiting the same oxidation potential for the ferrocene unit as **4**. In contrast, DPVs of **L1** and **L2** starting from −1.60 V showed no change compared to those starting from −0.30 V. Since the reduction potential of the terpyridine units in **L1** and **L2** is more anodic than those of **R1**, the 2 + 2 ladder frameworks seem to resist dissociation of the reduced coordination sites much more than **R1**, most likely due to cooperative effects. But when more negative DPV starting potentials of −1.80 V and −2.00 V were applied to **L1** and **L2**, the ferrocene potentials now showed up at 0.451 V for **L1** and 0.462 V for **L2** (Fig. 6). Under these conditions, as for **R1**, reduction seems to lead to a disintegration of the ladders. There are, however, differences between **L1** and **L2**. Upon starting the DPV investigation for **L1** at −1.80 V, the ladder showed disintegration as evidenced by an oxidation potential of the ferrocene units at 0.451 V. The sweep does not only entail reduction of the terpyridine, but also of the phenanthroline unit, thereby causing irreparable dissociation of the phen-Zn(II)-terpy coordination centres. **L2** proved to be less susceptible to negative starting potentials. Even when the DPV scan was initiated at −2.00 V, the oxidation potential of the ferrocenes emerged at 0.462 V. We assign this small shift of 10 mV tentatively to a partially broken ladder of **L2**. Due to its smaller size, ladder **L2** suffers probably less dissociation upon reduction than **L1**, as cooperative effects are more pronounced.

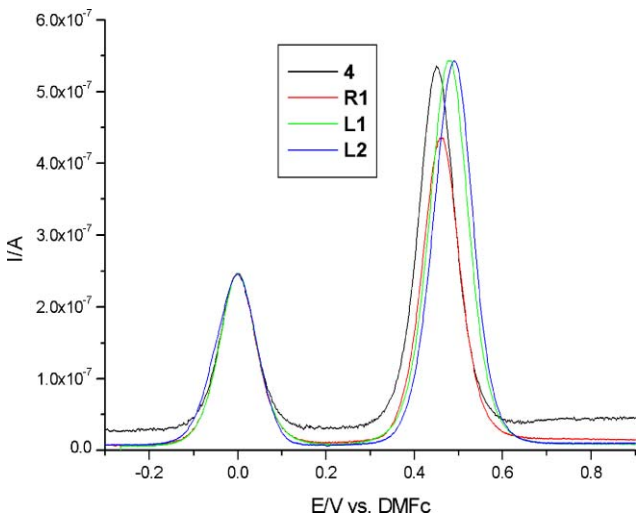

Fig. 5 DPVs of compounds **4**, **R1**, **L1** and **L2** recorded in 0.10 M $^{n}Bu_4NPF_6$ in acetonitrile. Step potential 2 mV, scan range from −0.30 V to 1.00 V.

Table 3 DPV measurements. Step potential 2 mV, scan range from −0.30 V to 1.00 V

Compound	**4**	**R1**	**L1**	**L2**
$E_{1/2}^{ox}$ ($Fc^{2+/3+}$)	0.452 V	0.462 V	0.480 V	0.491 V

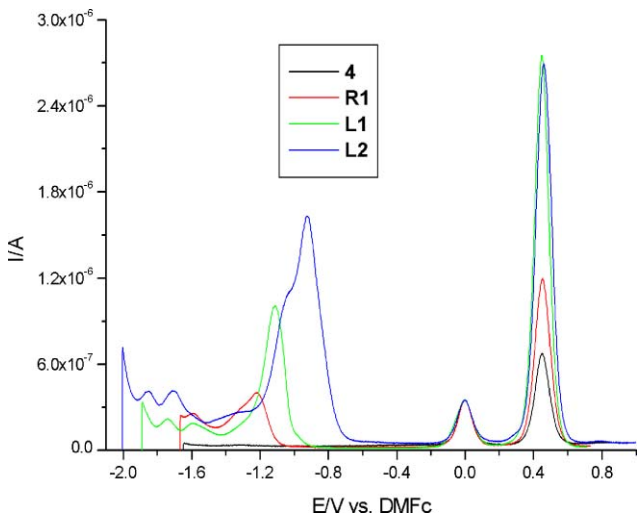

Fig. 6 DPVs of compounds **4**, **R1**, **L1** and **L2** recorded in 0.10 M $^{n}Bu_4NPF_6$ in acetonitrile. Step potential 2 mV, starting scan in between −2.00 and −1.60 V, finishing scan at 1.00 V.

Conclusion

Employing a directional approach using the HETTAP concept, we have achieved the synthesis of three internally functionalised supramolecular aggregates: the nanoscale rack **R1**, and nanoladders **L1** and **L2**, containing two and four ferrocenes, respectively. The redox potential of the ferrocene units in **R1** was slightly

anodically shifted by *ca.* 10 mV compared with that of **4**, due to the influence of the remote phen-Zn(II)-terpy coordination centre. In contrast, the ladder structure of **L1** and **L2** forces four ferrocene units into close proximity, thereby dramatically increasing their through-space interaction as demonstrated by the redox potential results. The redox potential series (*vs.* DMFc: $E_{1/2}$ = 0.462 V for **R1**, 0.480 V for **L1** and 0.491 V for **L2**), as determined by DPV, thus revealed convincingly the supramolecular effect on a redox process.

Experimental

All reagents were commercially available and used without further purification. Thin-layer chromatography was performed using silica gel 60 TLC plates (F_{254}, Merck). Silica gel (0.063–0.2 mm) was used for column chromatography. Confirmation of structures was obtained from ^{1}H-NMR and ^{13}C-NMR data (Bruker AC200 and Avance 400 spectrometer) using the deuterated solvent as the lock and residual solvent as the internal reference. The numbering of carbon atoms of molecular formulae as provided below is only used for the assignment and is not in accordance with the IUPAC nomenclature rules. Melting points were taken using the melting point apparatus of Dr Tottoli (Büchi) and are uncorrected. Electrospray mass spectra (ESI-MS) were recorded on a ThermoQuest LCQ Deca instrument. Infrared spectra were recorded on a Perkin Elmer 1750 FT-IR spectrometer. Cyclic voltagram (CV) and differential pulse voltammograms (DPV) were recorded on a Parstat 2273 instrument from Princeton Applied Research.

3-Ethynyl-2-(4-hydroxy-2,6-dimethylphenyl)-9-mesityl-[1,10]phenanthroline (2)

Compound **1**[19] (7.00 g, 10.4 mmol, 2-(4-triisopropylsilyloxy-2,6-dimethylphenyl)-9-mesityl-3-(trimethylsilylethynyl)-[1,10]phenanthroline) was dissolved in a mixture of methanol (100 mL) and THF (100 mL), and KOH (3 N in H_2O, 100 mL) was added slowly. After stirring for 24 h at room temperature, the solution was neutralised with sat. NH_4Cl and extracted with dichloromethane (200 mL). The organic layer was dried over $MgSO_4$. After removal of the solvent at reduced pressure, the crude product was recrystallised from dichloromethane to afford the product as a white solid (4.11 g, 9.28 mmol; 89%). Mp 290–291 °C. IR (KBr): $\tilde{\nu}$ = 3408 (w), 3312 (w), 2918 (w), 1616 (s), 1600 (s), 1583 (s), 1539 (w), 1506 (w), 1458 (s), 1395 (m), 1319 (s), 1152 (s), 1034 (m), 910 (m), 891 (w), 851 (s), 778 (w), 637 (s), 616 (m). ^{1}H-NMR (200 MHz, DMSO-d_6): δ = 1.86 (s, 6H, 7′-, 8′-H), 1.96 (s, 6H, 7‴-, 9‴-H), 2.29 (s, 3H, 8‴-H), 4.32 (s, 1H, 2′-H), 6.54 (s, 2H, 3′, 5′-H), 6.97 (s, 2H, 3‴-, 5‴-H), 7.68 (d, J = 8.1 Hz, 1H, 8-H), 8.03 (d, J = 8.9 Hz, 1H, 6-H), 8.10 (d, J = 8.9 Hz, 1H, 5-H), 8.56 (d, J = 8.1 Hz, 1H, 7-H), 8.77 (s, 1H, 4-H), 9.35 (br s, 1H, 9′-H). ^{13}C-NMR (50 MHz, DMSO-d_6): δ = 19.7, 19.8, 20.8, 80.6, 85.9, 113.9, 118.7, 121.9, 125.0, 125.7, 126.4, 127.1, 127.5, 128.1, 130.7, 135.1, 136.6, 136.9, 137.8, 140.3, 144.3, 145.0, 156.8, 159.6, 160.9. ESI-MS Calcd for $[M + H]^+$: m/z 443.2, Found: m/z 443.2. Anal calcd for $C_{31}H_{26}N_2O{\cdot}1.5H_2O$: C, 79.29; H, 6.22; N, 5.97; found: C, 79.04; H, 5.96; N, 6.16.

1,4-Bis[(2-(4-hydroxy-2,6-dimethylphenyl)-9-mesityl-[1,10]phenanthroline-3-ylethynyl]benzene (3)

Phenanthroline **2** (91.2 mg, 206 μmol), 1,4-diiodobenzene (34.0 mg, 103 μmol) and $[Pd(PPh_3)_4]$ (11.5 mg, 10.0 μmol) were dissolved in dry DMF (15 mL) and dry triethylamine (15 mL). After deoxygenating the reaction mixture with nitrogen for 15 min, it was heated to 60 °C for 4 h. Then the solvents were removed at reduced pressure, and the residue was washed with water (30 mL) and dichloromethane (30 mL) to afford the crude product. It was recrystallised from DMF to afford a light yellow solid (88.9 mg, 92.7 μmol, 90%). Mp >300 °C. IR (KBr): $\tilde{\nu}$ = 3363 (w), 2963 (w), 2920 (w), 2212 (w), 1614 (s), 1586 (s), 1506 (m), 1458 (s), 1396 (m), 1317 (s), 1159 (s), 1034 (w), 909 (m), 889 (m), 850 (s), 776 (w), 639 (m). ^{1}H-NMR (200 MHz, DMF-d_7): δ = 2.02 (s, 12H, 7′-, 8′-H), 2.05 (s, 12H, 7‴-, 9‴-H), 2.32 (s, 6H, 8‴-H), 6.70 (s, 4H, 3′, 5′-H), 6.99 (s, 4H, 3‴-, 5‴-H), 7.30 (s, 4H, 4′-, 5′-H), 7.78 (d, J = 8.1 Hz, 2H, 8-H), 8.15 (d, J = 8.8 Hz, 2H, 6-H), 8.20 (d, J = 8.8 Hz, 2H, 5-H), 8.66 (d, J = 8.1 Hz, 2H, 7-H), 8.87 (s, 2H, 4-H), 9.56 (br s, 2H, 9′-H). ^{13}C-NMR (50 MHz, DMSO-d_6): δ = 19.7, 21.0, 21.7, 80.6, 85.6, 113.9, 114.0, 118.7, 121.9, 125.0, 125.7, 126.4, 127.2, 127.5, 128.1, 128.2, 130.7, 135.1, 136.6, 136.9, 137.8, 140.5, 144.3, 145.0, 156.8, 159.6, 160.9. ESI-MS Calcd for $[M + H]^+$: m/z 959.4, Found: m/z 959.6; ESI-MS Calcd for $[M + 2H]^{2+}$: m/z 480.2, Found: m/z 480.3. Anal calcd for $C_{68}H_{54}N_4O_2{\cdot}H_2O$: C, 83.58; H, 5.78; N, 5.73; found: C, 83.96; H, 5.71; N, 5.81.

1,4-Bis{2-[2,6-dimethyl-4-(6-ferrocenylhexyloxy)phenyl]-9-mesityl-[1,10]phenanthroline-3-ylethynyl}benzene (5)

Compound **3** (100 mg, 104 μmol) was dissolved in dry DMF (30 mL). NaH (60% in mineral oil, 60 mg, 2.50 mmol) was added and the mixture was then stirred for 1 h at room temperature. After addition of 6-bromohexylferrocene (**4**)[20] (140 mg, 400 μmol), the reaction mixture was heated to 80–90 °C (oil bath temperature) for 24 h. The reaction was quenched by careful addition of water (50 mL) and neutralised with saturated NH_4Cl solution. After extraction with DCM (3 × 50 mL), the organic layer was dried over $MgSO_4$. Then the solvent was removed at reduced pressure and the crude product was purified by column chromatography (SiO_2, dichloromethane) to afford the product as a yellow solid (124 mg, 82.9 μmol, 80%). Mp >300 °C. IR (KBr): $\tilde{\nu}$ = 2924 (s), 2855 (m), 2210 (w), 1605 (s), 1583 (m), 1500 (w), 1459 (s), 1396 (w), 1316 (m), 1160 (s), 1105 (w), 1071 (w), 887 (m), 849 (s), 637 (w), 485 (w). ^{1}H-NMR (400 MHz, CD_2Cl_2): δ = 1.40–1.61 (m, 12H, 3‴-, 4‴-, 5‴-H), 1.80–1.87 (m, 4H, 2‴-H), 2.06 (s, 12H, 7′-, 8′-H), 2.07 (s, 12H, 7″-, 9″-H), 2.34 (s, 6H, 8″-H), 2.36 (t, J = 7.6 Hz, 4H, 6‴-H), 4.00–4.07 (m, 12H, 1‴-, 8‴-, 9‴-H), 4.08 (s, 10H, 10‴-H), 6.72 (s, 4H, 3′-, 5′-H), 6.97 (s, 4H, 3″-, 5″-H), 7.15 (s, 4H, 4′-, 5′-H), 7.57 (d, J = 8.1 Hz, 2H, 8-H), 7.86 (d, J = 8.8 Hz, 2H, 6-H), 7.91 (d, J = 8.8 Hz, 2H, 5-H), 8.33 (d, J = 8.1 Hz, 2H, 7-H), 8.49 (s, 2H, 4-H). ^{13}C-NMR (100 MHz, CD_2Cl_2): δ = 20.3, 20.4, 21.2, 26.3, 29.6, 29.7, 29.8, 31.5, 67.3, 68.3, 68.4, 68.8, 89.3, 89.8, 94.5, 113.6, 120.0, 123.2, 125.2, 125.9, 127.2, 127.3, 128.0, 128.6, 131.8, 132.9, 136.0, 136.4, 137.8, 138.0, 138.4, 139.0, 145.4, 146.4, 159.0, 160.9, 161.8. ESI-MS Calcd for $[M + H]^+$: m/z 1495.6, Found: m/z 1495.9, Calcd for $[M + 2H]^{2+}$: m/z = 748.3, Found: m/z = 748.4. Anal calcd for $C_{100}H_{94}Fe_2N_4O_2$: C, 80.31; H, 6.34; N, 3.75; found: C, 80.10; H, 6.34; N, 3.71.

Nanorack R1

The ferrocene ligand **5** (5.00 mg, 3.34 μmol) and $Zn(CF_3SO_3)_2$ (2.43 mg, 6.68 μmol) were dissolved in deuterated dichloromethane–methanol (8 : 2, 0.6 mL),[14] and terpyridine (**8**) (1.54 mg, 6.68 μmol) was added. The resulting suspension was heated for a few minutes until a clear solution had formed. It was analysed by ESI-MS, ^{1}H-, ^{13}C-NMR and elemental analysis without any further purification. Mp >300 °C. IR (KBr): $\tilde{\nu}$ = 3422 (w), 3081 (w), 2927 (m), 2855 (m), 2213 (w), 1602 (m), 1579 (m), 1479 (w), 1456 (m), 1407 (w), 1322 (w), 1262 (s), 1223 (m), 1155 (s), 1031 (s), 854 (w), 638 (s). ^{1}H-NMR (400 MHz, CD_2Cl_2–CD_3OD (8 : 2)): δ = 1.12 (s, 24H, 7′-, 8′-, 7″-, 9″-H), 1.31–1.37 (m, 8H, 3‴-, 4‴-H), 1.48–1.60 (m, 8H, 2‴-, 5‴-H), 1.79 (s, 6H, 8″-H), 2.25 (br s, 4H, 6‴-H), 3.46 (t, J = 6.3 Hz, 4H, 1‴-H), 4.22 (br s, 18H, 8‴-, 9‴-, 10‴-H), 5.86 (s, 4H, 3′-, 5′-H), 6.18 (s, 4H, 3″-, 5″-H), 7.00 (s, 4H, 4′-, 5′-H), 7.53 (ddd, J = 7.7 Hz, 5.1 Hz, 1.0 Hz, 4H, b-H), 7.76 (dd, J = 5.1 Hz, 1.0 Hz, 4H, a-H), 8.03 (d, J = 8.1 Hz, 2H, 8-H), 8.27 (dt, J = 7.7 Hz, 1.6 Hz, 4H, c-H), 8.42–8.50 (m, 14H, d-, e-, f-, 5-, 6-H), 9.04 (d, J = 8.1 Hz, 2H, 7-H), 9.07 (s, 2H, 4-H). ^{13}C-NMR (100 MHz, CD_2Cl_2–CD_3OD (8 : 2)): δ = 19.2, 19.4, 20.7, 26.2, 29.3, 29.6, 29.7, 31.2, 68.2, 68.4 (Fc), 69.3 (Fc), 70.0 (Fc), 86.2, 97.8, 112.7, 122.7, 123.1, 123.6, 124.5, 127.9, 128.0, 128.2, 128.5, 129.0, 129.1, 129.6, 130.0, 132.1, 134.7, 135.3, 137.3, 139.8, 140.5, 141.4, 143.1, 143.2, 144.2, 144.7, 146.8, 147.6, 149.5, 160.1, 161.6, 162.8. ESI-MS: calcd. for $[M - 4OTf^-]^{4+}$: m/z 523.2, found: m/z 523.2, calcd. for $[M - 3OTf^-]^{3+}$: m/z 747.3, found: m/z 746.9, calcd. for $[M - 2OTf^-]^{2+}$: m/z 1195.5, found: m/z 1195.4. Anal calcd for $C_{134}H_{116}F_{12}Fe_2N_{10}O_{14}S_4Zn_2{\cdot}0.5CH_2Cl_2$: C, 59.14; H, 4.32; N, 5.13; S, 4.70; found: C, 59.16; H, 4.16; N, 5.10; S, 4.65.

Nanoladder L1

Ligand **5** (5.00 mg, 3.34 μmol) and $Zn(CF_3SO_3)_2$ (2.43 mg, 6.68 μmol) were dissolved in deuterated dichloromethane–methanol (8 : 2, 0.6 mL),[14] and bisterpyridine **6** (2.33 mg, 3.34 μmol) was added. The resulting suspension was heated for a few minutes until a clear solution had formed. It was analysed by ESI-MS, ^{1}H-, ^{13}C-NMR and elemental analysis without any further purification. Mp >300 °C. $\tilde{\nu}$ = 3083 (w), 2926 (m), 2854 (m), 2211 (w), 1603 (s), 1577 (m), 1476 (m), 1420 (w), 1261 (s), 1223 (m), 1160 (s), 1031 (s), 852 (w), 797 (w), 638 (s). ^{1}H-NMR (400 MHz, CD_2Cl_2–CD_3OD (8 : 2)): δ = 1.18 (s, 24H, 7′-, 8′-H), 1.22 (s, 24H, 7″-, 9″-H), 1.17–1.40 (m, 24H, 2‴-, 3‴-, 4‴-H), 1.54 (br s, 8H, 5‴-H), 1.90 (s, 12H, 8″-H), 2.19–2.26 (m, 32H, 6‴-, g-H), 3.53 (t, J = 6.3 Hz, 8H, 1‴-H), 4.24 (br s, 36H, 8‴-, 9‴-, 10‴-H), 5.93 (s, 8H, 3′-, 5′-H), 6.27 (s, 8H, 3″-, 5″-H), 7.05 (s, 8H, 4′-, 5′-H), 7.55–7.58 (m, 16H, b-, f-H), 7.81 (d, J = 4.8 Hz, 8H, a-H), 8.05 (d, J = 8.3 Hz, 4H, 8-H), 8.24–8.28 (m, 16H, c-, e-H), 8.40 (d, J = 8.1 Hz, 8H, d-H), 8.48 (d, J = 9.4 Hz, 4H, 6-H), 8.53 (d, J = 9.4 Hz, 4H, 5-H), 9.08 (d, J = 8.3 Hz, 4H, 7-H), 9.16 (s, 4H, 4-H). ^{13}C-NMR (100 MHz, CD_2Cl_2–CD_3OD (8 : 2)): δ = 19.3, 19.6, 20.9, 21.0, 26.1, 29.4, 29.6, 29.7, 31.2, 68.4, 69.5 (Fc), 86.2, 90.2, 97.8, 112.8, 119.3, 122.4, 122.8, 123.6, 124.1, 124.6, 124.8, 128.0, 128.5, 128.9, 129.1, 129.3, 129.7, 130.0, 131.7, 132.2, 134.7, 135.5, 135.9, 137.1, 137.6, 140.0, 140.4, 141.6, 143.4, 144.7, 146.5, 148.0, 149.6, 158.7, 160.3, 161.8, 162.7. ESI-MS: calcd. for $[M - 8OTf^-]^{8+}$: m/z 580.8, found: m/z 580.7, calcd. for $[M - 7OTf^-]^{7+}$: m/z 685.0, found: m/z 685.0, calcd. for $[M - 6OTf^-]^{6+}$: m/z 824.1, found: m/z 823.9, calcd. for $[M - 5OTf^-]^{5+}$: m/z 1018.7, found: m/z 1018.5, calcd. for $[M - 4OTf^-]^{4+}$: m/z 1310.6, found: m/z 1310.6, calcd. for $[M - 3OTf^-]^{3+}$: m/z 1797.2, found: m/z 1796.9. Anal calcd for $C_{304}H_{260}F_{24}Fe_4N_{20}O_{28}S_8Zn_4{\cdot}3CH_2Cl_2$: C, 60.51; H, 4.40; N, 4.60; S, 4.21; found: C, 60.78; H, 4.24; N, 4.51; S, 4.33.

Nanoladder L2

Ligand **5** (5.00 mg, 3.34 μmol) and $Zn(CF_3SO_3)_2$ (2.43 mg, 6.68 μmol) were dissolved in deuterated dichloromethane–methanol (8 : 2, 0.6 mL),[14] then bisterpyridine **7** (1.81 mg, 3.34 μmol) was added. The resulting suspension was heated for a few minutes until a clear solution had formed. It was analysed by ESI-MS, ^{1}H-, ^{13}C-NMR and elemental analysis without any further purification. Mp >300 °C. $\tilde{\nu}$ = 3402 (w), 3094 (w), 2922 (m), 2855 (m), 2212 (w), 1605 (s), 1577 (m), 1477 (w), 1459 (m), 1400 (w), 1279 (s), 1254 (s), 1161 (s), 1031 (s), 854 (w), 639 (s). ^{1}H-NMR (400 MHz, CD_2Cl_2–CD_3OD (8 : 2)): δ = 1.10 (s, 24H, 7′-, 8′-H), 1.16 (s, 24H, 7″-, 9″-H), 1.12–1.37 (m, 32H, 2‴-, 3‴-, 4‴-, 5‴-H), 1.72 (s, 12H, 8″-H), 2.10 (br s, 8H, 6‴-H), 3.43 (t, J = 6.4 Hz, 8H, 1‴-H), 3.86–3.98 (m, 36H, 8‴-, 9‴-, 10‴-H), 5.91 (s, 8H, 3′-, 5′-H), 6.21 (s, 8H, 3″-, 5″-H), 7.00 (s, 8H, 4′-, 5′-H), 7.53 (td, J = 5.1 Hz, 1.2 Hz, 8H, b-H), 7.76 (d, J = 5.1 Hz, 8H, a-H), 8.08 (d, J = 8.1 Hz, 4H, 8-H), 8.30 (td, J = 8.1 Hz, 1.2 Hz, 8H, c-H), 8.48 (d, J = 8.8 Hz, 4H, 6-H), 8.52 (d, J = 8.8 Hz, 4H, 5-H), 8.60 (s, 8H, e-H), 8.92 (d, J = 8.1 Hz, 8H, d-H), 9.03 (s, 8H, f-H), 9.08 (d, J = 8.1 Hz, 4H, 7-H), 9.21 (s, 4H, 4-H). ^{13}C-NMR (100 MHz, CD_2Cl_2/CD_3OD (8:2)): δ = 19.4, 19.5, 20.7, 25.4, 26.0, 29.5, 29.9, 31.3, 67.7, 68.3, 68.6, 70.0, 86.4, 97.79, 101.4, 109.2, 112.9, 116.4, 119.5, 120.6, 122.8, 124.5, 125.9, 128.1, 128.5, 129.3, 130.1, 132.4, 134.9, 135.4, 137.6, 138.0, 140.0 (2C), 140.8, 141.5, 142.2, 143.5, 144.7, 146.8, 147.3 (2C), 148.5, 149.4, 155.5 (2C), 161.4, 161.9, 162.8. ESI-MS: calcd. for $[M - 8OTf^-]^{8+}$: m/z 541.7, found: m/z 541.6, calcd. for $[M - 7OTf^-]^{7+}$: m/z 640.4, found: m/z 640.3, calcd. for $[M - 6OTf^-]^{6+}$: m/z 772.0, found: m/z 772.2, calcd. for $[M - 5OTf^-]^{5+}$: m/z 956.2, found: m/z 955.9, calcd. for $[M - 4OTf^-]^{4+}$: m/z 1232.5, found: m/z 1232.2, calcd. for $[M - 3OTf^-]^3$ m: m/z 1693.1, found: m/z 1692.8. Anal calcd for $C_{280}H_{236}F_{24}Fe_4N_{20}O_{28}S_8Zn_4{\cdot}CH_2Cl_2$: C, 60.15; H, 4.28; N, 4.99; S, 4.57; found: C, 59.89; H, 4.16; N, 4.87; S, 4.77.

Acknowledgements

We are grateful to the Deutsche Forschungsgemeinschaft and the Fonds der Chemischen Industrie. In addition, we are indebted to Dr Mal for providing us with ligand **6**.

References

1 M. Schmittel and V. Kalsani, *Top. Curr. Chem.*, 2005, **245**, 1–53.
2 J.-M. Lehn, *Supramolecular Chemistry: Concepts and Perspectives*, VCH, Weinheim, 1995.
3 L. J. Prins, D. N. Reinhoudt and P. Timmerman, *Angew. Chem., Int. Ed.*, 2001, **40**, 2382–2426.
4 M. Fujita, D. Oguro, M. Miyazawa, H. Oka, K. Yamaguchi and K. Ogura, *Nature*, 1995, **378**, 469–471; B. J. Holliday and C. A. Mirkin, *Angew. Chem., Int. Ed.*, 2001, **40**, 2022–2043; S. R. Seidel and P. J. Stang, *Acc. Chem. Res.*, 2002, **35**, 972–983; F. Würthner, C.-C. You and C. R. Saha-Moeller, *Chem. Soc. Rev.*, 2004, 133–146; M. Ruben, J. Rojo, F. J. Romero-Salguero, L. H. Uppadine and J.-M. Lehn, *Angew.*

Chem., Int. Ed., 2004, **43**, 3644–3662; M. Fujita, M. Tominaga, A. Hori and B. Therrien, *Acc. Chem. Res.*, 2005, **38**, 371–380.
5 M. Schmittel, R. S. K. Kishore and J. W. Bats, *Org. Biomol. Chem.*, 2007, **5**, 78–86 and references cited therein.
6 (*a*) F. D'Souza, P. M. Smith, S. Gadde, A. L. McCarty, M. J. Kullman, M. E. Zandler, M. Itou, Y. Araki and O. Ito, *J. Phys. Chem. B*, 2004, **108**, 11333–11343; (*b*) H. Nakagawa, K. Ogawa, A. Satake and Y. Kobuke, *Chem. Commun.*, 2006, 1560–1562.
7 P. J. Stang, B. Olenyuk, J. Fan and A. M. Arif, *Organometallics*, 1996, **15**, 904–908; P. J. Stang, D. H. Cao, K. Chen, G. M. Gray, D. C. Muddiman and R. D. Smith, *J. Am. Chem. Soc.*, 1997, **119**, 5163–5168; S.-S. Sun, J. A. Anspach and A. J. Lees, *Inorg. Chem.*, 2002, **41**, 1862–1869.
8 R. V. Slone and J. T. Hupp, *Inorg. Chem.*, 1997, **36**, 5422–5423.
9 C. M. Drain and J.-M. Lehn, *J. Chem. Soc., Chem. Commun.*, 1994, 2313–2315.
10 J. Fan, J. A. Whiteford, B. Olenyuk, M. D. Levin and P. J. Stang, *J. Am. Chem. Soc.*, 1999, **121**, 2741–2752.
11 C.-C. You and F. Würthner, *J. Am. Chem. Soc.*, 2003, **125**, 9716–9725; F. Würthner and A. Sautter, *Org. Biomol. Chem.*, 2003, 240–243.
12 M. Tominaga, K. Suzuki, M. Kawano, T. Kusukawa, T. Ozeki, S. Sakamoto, K. Yamaguchi and M. Fujita, *Angew. Chem., Int. Ed.*, 2004, **43**, 5621–5625; M. Tominaga, K. Suzuki, T. Murase and M. Fujita, *J. Am. Chem. Soc.*, 2005, **127**, 11950–11951; S. Sato, J. Iida, K. Suzuki, M. Kawano, T. Ozeki and M. Fujita, *Science*, 2006, **313**, 1273–1276.
13 P. N. W. Baxter, G. S. Hanan and J.-M. Lehn, *Chem. Commun.*, 1996, 2019–2020.
14 M. Schmittel, V. Kalsani, R. S. P. Kishore, J. W. Bats and H. Cölfen, *J. Am. Chem. Soc.*, 2005, **127**, 11544–11545. The HETTAP strategy makes use of steric and electronic effects originating from bulky aryl substituents at the bisimine coordination sites (as seen in **5**) to control the coordination equilibrium both kinetically and thermodynamically. The steric stoppers at the coordination sites (the 2- and 9-positions) of bisphenanthroline prevent any competitive homoleptic combination of itself, therefore leading to just hetero-combinations.
15 M. Schmittel, V. Kalsani, P. Mal and J. W. Bats, *Inorg. Chem.*, 2006, **45**, 6370–6377.
16 M. Schmittel, C. Michel, A. Wiegrefe and V. Kalsani, *Synthesis*, 2001, 1561–1567.
17 For an alternative strategy to terpyrine phenanthroline complexes, see: C. Hamann, J.-M. Kern and J.-P. Sauvage, *Inorg. Chem.*, 2003, **42**, 1877–1883.
18 F. A. Cotton, C. Lin and C. A. Murillo, *Acc. Chem. Res.*, 2001, **34**, 759–771.
19 M. Schmittel, V. Kalsani, F. Jäckel, J. P. Rabe, J. W. Bats and D. Fenske, *Eur. J. Org. Chem.*, 2006, 3079–3086.
20 K. K.-W. Lo, D. C.-M. Ng, J. S.-Y. Lau, R. S.-S. Wu and P. K.-S. Lam, *New J. Chem.*, 2003, **27**, 274–279.
21 S.-H. Hwang, C. N. Moorefield, F. R. Fronczek, O. Lukoyanova, L. Echeguyen and G. R. Newkome, *Chem. Commun.*, 2005, 713–715.
22 Similar anodic shifts have been reported for inclusion complexes of ferrocenes in a supramolecular atmosphere: A. E. Kaifer, *Acc. Chem. Res.*, 1999, **32**, 62; C. M. Cardona, S. Mendoza and A. E. Kaifer, *Chem. Soc. Rev.*, 2000, **29**, 37; D. L. Stone, D. K. Smith and P. T. McGrail, *J. Am. Chem. Soc.*, 2002, **124**, 856–864; W.-Y. Sun, T. Kusukawa and M. Fujita, *J. Am. Chem. Soc.*, 2002, **124**, 11570–11571.